Real-time fluorescence lifetime imaging system with a 32 × 32 0.13μm CMOS low dark-count single-photon avalanche diode array

Day-Uei Li[1,*], Jochen Arlt[2], Justin Richardson[1,3], Richard Walker[1,3], Alex Buts[1], David Stoppa[4], Edoardo Charbon[5], and Robert Henderson[1]

[1]*Institute for Integrated Micro and Nano Systems, Joint Research Institute for Signal & Image Processing/Integrated Systems/Energy/Civil and Environmental Engineering, School of Engineering, University of Edinburgh, Faraday Building, The King's Buildings, Edinburgh EH9 3JL, Scotland, UK*
[2]*School of Physics and Astronomy, University of Edinburgh, Joseph Black Building, The Kings' Buildings, Edinburgh EH9 3JJ, Scotland, UK*
[3]*Imaging Division, ST Microelectronics, Edinburgh EH12 7BF, Scotland, UK*
[4]*Smart Optical Sensors and Interfaces, Fondazione Bruno Kessler, Trento, Italy*
[5]*EEMCS Faculty, Delft University of Technology, Mekelweg 4, 2628CD Delft, Neitherlands*
**David.Li@ed.ac.uk*

Abstract: A compact real-time fluorescence lifetime imaging microscopy (FLIM) system based on an array of low dark count 0.13μm CMOS single-photon avalanche diodes (SPADs) is demonstrated. Fast background-insensitive fluorescence lifetime determination is achieved by use of a recently proposed algorithm called 'Integration for Extraction Method' (IEM) [J. Opt. Soc. Am. A **25**, 1190 (2008)]. Here, IEM is modified for a wider resolvability range and implemented on the FPGA of the new SPAD array imager. We experimentally demonstrate that the dynamic range and accuracy of calculated lifetimes of this new camera is suitable for widefield FLIM applications by imaging a variety of test samples, including various standard fluorophores covering a lifetime range from 1.6ns to 16ns, microfluidic mixing of fluorophore solutions, and living fungal spores of *Neurospora Crassa*. The calculated lifetimes are in a good agreement with literature values. Real-time fluorescence lifetime imaging is also achieved, by performing parallel 32 × 16 lifetime calculations, realizing a compact and low-cost FLIM camera and promising for bigger detector arrays.

OCIS codes: (030.5260) Coherence and statistical optics; Photon counting; (040.1345) Detectors: Avalanche diodes (APDs); (110.0180) Imaging systems: microscopy; (170.2520) Medical optics and biotechnology: fluorescence microscopy; (170.3650) Medical optics and biotechnology: Lifetime-based sensing; (170.6920) Medical optics and biotechnology: Time-resolved imaging

References and links

1. J. R. Lakowicz, *Principles of Fluorescence Spectroscopy*, 3rd ed. Kluwer (Academic/Plenum Publishers, New York, 2006).
2. P. I. H. Bastiaens, and A. Squire, "Fluorescence lifetime imaging microscopy: spatial resolution of biochemical processes in the cell," Trends Cell Biol. **9**(2), 48–52 (1999).
3. M. Gersbach, D. L. Boiko, C. Niclass, C. C. Petersen, and E. Charbon, "Fast-fluorescence dynamics in nonratiometric calcium indicators," Opt. Lett. **34**(3), 362–364 (2009).
4. A. Draaijer, R. Sanders, and H. C. Gerritsen, "Fluorescence lifetime imaging, a new tool in confocal microscopy," in *Handbook of Biological Confocal Microscopy*, J. P. Pawley, Ed., Plenum Press, 491–505 (1995).
5. M. Gersbach, J. Richardson, E. Mazaleyrat, S. Hardillier, C. Niclass, R. Henderson, L. Grant, and E. Charbon, "A low-noise single photon detector implemented in a 130nm CMOS imaging process," Solid-State Electron. **53**(7), 803–808 (2009).
6. R. K. Henderson, J. Richardson, and L. Grant, "Reduction of band-to-band tunneling in deep-submicron CMOS single photon avalanche photodiodes," presented at the International Image Sensor Workshop (IISW 2009), Bergen, Norway, 26–28 June 2009.

#123554 - $15.00 USD Received 12 Feb 2010; revised 22 Mar 2010; accepted 22 Mar 2010; published 3 May 2010

http://www.imagesensors.org/Past%20Workshops/2009%20Workshop/2009%20Papers/022_paper_henderson_univ_edinburgh_spad_final.pdf.
7. J. A. Richardson, L. A. Grant, and R. K. Henderson, "Low dark count single-photon avalanche diode structure compatible with standard nanometer scale CMOS technology," IEEE Photon. Technol. Lett. **21**(14), 1020–1022 (2009).
8. B. Rae, C. Griffin, K. Muir, J. Girkin, E. Gu, D. Renshaw, E. Charbon, M. Dawson, and R. Henderson, "A microsystem for time-resolved fluorescence analysis using CMOS single-photon avalanche diodes and micro-LEDs," in *Proceedings of IEEE Conference on Solid State Circuits* (IEEE, New York, 2008), pp. 166–167. *http://infoscience.epfl.ch/record/125270/files/isscc08_rh_pub.pdf*.
9. J. Richardson, R. Walker, L. Grant, D. Stoppa, F. Borghetti, E. Charbon, M. Gersbach, and R. Henderson, "A 32x32 50ps resolution 10 bit time to digital converter array in 130nm CMOS for time correlated imaging," in *Proceedings of IEEE Conference on Custom Integrated Circuits* (IEEE, New York, 2009), pp. 77–80. *http://ieeexplore.ieee.org/stamp/stamp.jsp?tp=&arnumber=5280890*.
10. P. Hall, and B. Selinger, "Better estimates of exponential decay parameters," J. Phys. Chem. **85**(20), 2941–2946 (1981).
11. J. A. Jo, Q. Fang, and L. Marcu, "Ultrafast method for the analysis of fluorescence lifetime imaging microscopy data based on the Laguerre expansion technique," IEEE J. Sel. Top. Quantum Electron. **11**(4), 835–845 (2005).
12. S. W. Magennis, E. M. Graham, and A. C. Jones, "Quantitative spatial mapping of mixing in microfluidic systems," Angew. Chem. Int. Ed. **44**(40), 6512–6516 (2005).
13. A. V. Agronskaia, L. Tertoolen, and H. C. Gerritsen, "High frame rate fluorescence lifetime imaging," J. Phys. D Appl. Phys. **36**(14), 1655–1662 (2003).
14. D.-U. Li, E. Bonnist, D. Renshaw, and R. Henderson, "On-chip time-correlated fluorescence lifetime extraction algorithms and error analysis," J. Opt. Soc. Am. A **25**(5), 1190–1198 (2008).
15. D.-U. Li, R. Walker, J. Richardson, B. Rae, A. Buts, D. Renshaw, and R. Henderson, "Hardware implementation and calibration of background noise for an integration-based fluorescence lifetime sensing algorithm," J. Opt. Soc. Am. A **26**(4), 804–814 (2009).
16. R. M. Ballew, and J. N. Demas, "An error analysis of the rapid lifetime determination method for the evaluation of single exponential decays," Anal. Chem. **61**(1), 30–33 (1989).
17. D. S. Elson, I. Munro, J. Requejo-Isidro, J. McGinty, C. Dunsby, N. Galletly, G. W. Stamp, M. A. A. Neil, M. J. Lever, P. A. Kellett, A. Dymoke-Bradshaw, J. Hares, and P. M. W. French, "Real-time time-domain fluorescence lifetime imaging including single-shot acquisition with a segmented optical image intensifier," N. J. Phys. **6**, 180 (2004).
18. D.-U. Li, B. Rae, E. Bonnist, D. Renshaw, and R. Henderson, "On-chip fluorescence lifetime extraction using synchronous gating scheme-Theoretical error analysis and practical implementation," in *Proceedings of Int. Conf. Bio-inspired Systems and Signal processing, INSTICC*, (Academic, Lisbon, Portugal, 2008), pp. 171–176. *http://www.biosignals.biostec.org/Abstracts/2008/BIOSIGNALS_2008_Abstracts.htm*.
19. C. Moore, S. P. Chan, J. N. Demas, and B. A. DeGraff, "Comparison of methods for rapid evaluation of lifetimes of exponential decays," Appl. Spectrosc. **58**(5), 603–607 (2004).
20. W. Trabesinger, C. G. Hübner, B. Hecht, and T. P. Wild, "Continuous real-time measurement of fluorescence lifetime," Rev. Sci. Instrum. **73**(8), 3122–3124 (2002).
21. H. P. Good, A. J. Kallir, and U. P. Wild, "Comparison of fluorescence lifetime fitting techniques," J. Phys. Chem. **88**(22), 5435–5441 (1984).
22. P. C. Schneider, and R. M. Clegg, "Rapid acquisition, analysis, and display of fluorescence lifetime-resolved images for real-time applications," Rev. Sci. Instrum. **68**(11), 4107–4119 (1997).
23. J. Mizeret, T. Stepinac, M. Hansroul, A. Studzinski, H. van den Bergh, and G. Wagnières, "Instrumentation for real-time fluorescence lifetime imaging in endoscopy," Rev. Sci. Instrum. **70**(12), 4689–4701 (1999).
24. J. Philips, and K. Carlsson, "Theoretical investigation of the signal-to-noise ratio in fluorescence lifetime imaging," J. Opt. Soc. Am. A **20**(2), 368–379 (2003).
25. M. J. Booth, and T. Wilson, "Low-cost, frequency-domain, fluorescence lifetime confocal microscopy," J. Microsc. **214**(1), 36–42 (2004).
26. A. D. Elder, S. M. Matthews, J. Swartling, K. Yunus, J. H. Frank, C. M. Brennan, A. C. Fisher, and C. F. Kaminski, "Application of frequency-domain Fluorescence Lifetime Imaging Microscopy as a quantitative analytical tool for microfluidic devices," Opt. Express **14**(12), 5456–5467 (2006), http://www.opticsexpress.org/abstract.cfm?URI=oe-14-12-5456.
27. R. A. Colyer, C. Lee, and E. Gratton, "A novel fluorescence lifetime imaging system that optimizes photon efficiency," Microsc. Res. Tech. **71**(3), 201–213 (2008).
28. P. Alfke, *Efficient Shift Registers, LFSR Counters, and Long Pseudo-Random Sequence Generators*, XAPP052, Application Note, Xilinx, Inc., San Jose, CA 95124–3400 (1996).
29. S. Donati, G. Martini, and M. Norgia, "Microconcentrators to recover fill-factor in image photodetectors with pixel on-board processing circuits," Opt. Express **15**(26), 18066–18075 (2007), http://www.opticsinfobase.org/abstract.cfm?uri=oe-15-26-18066.

#123554 - $15.00 USD Received 12 Feb 2010; revised 22 Mar 2010; accepted 22 Mar 2010; published 3 May 2010

1. Introduction

Fluorescence based imaging techniques have become an essential tool for a large variety of disciplines, ranging from cell-biology, medical diagnosis, and pharmacological development to physical sciences [1]. Fluorescent labeling of samples allows high contrast imaging of spatial structures simply by recording the fluorescence intensity. However, if more quantitative information for physiological parameters such as pH, Ca^{2+}, and pO_2 etc. is required, techniques based on fluorescence lifetime rather than just intensity are much more appropriate [2,3]. Fluorescence lifetime is independent of the probe concentration and thus avoids many of the uncertainties, such as probe uptake and/or labeling efficiency, variations in excitation illumination etc., that make quantitative analysis of fluorescence intensity images very difficult.

There is a vast choice of implementations for fluorescence lifetime imaging available, both in the frequency and time domain [4]. Despite the fact that technology has matured in recent years, typical fluorescence lifetime imaging microscopy (FLIM) setups are still expensive and cumbersome. Fast pulsed lasers (either Ti-Sapphire laser for mutiphoton excitation or pulsed laser diodes for direct excitation) have to be coupled into the microscope and typically need to be scanned across the sample for confocal detection with a photomultiplier tube (PMT) coupled to a time-correlated single-photon counting (TCSPC) card. Often, the fluorescence lifetime is not displayed immediately but only extracted from the recorded fluorescence decay histograms by a separate piece of software. Clinical and commercial applications, on the other hand, increasingly demand compact, high-speed, and portable system-on-chip FLIM solutions which are robust and easy to operate. Thanks to the progress of semiconductor technology it is now possible to achieve high accuracy time resolution, high sensitivity, low cost, compactness, and high-throughput with parallelism by exploiting low dark count CMOS SPAD detectors [5–7] or SPAD arrays [8,9] to replace PMTs and by bump-bonding micro-pixilated light-emitting diodes (LEDs) to replace lasers [8].

For fast imaging, a remaining challenge is that the excessive computational demands of available lifetime analysis software such as the iterative least-square method or maximum-likelihood-estimation (MLE) [10] render real-time imaging impossible. A new FLIM algorithm considering the instrument response based on the Laguerre expansion technique [11] speeds up lifetime calculations but the computation time increases with imager size. In many applications such as microfluidic mixing [12], clinical applications, and exploratory biological experiments, however, it is desirable to monitor the instantaneous bio-chemical interactions to provide quick feedback to corresponding manipulations. The demand has driven the recent development of non-iterative, compact, and high-speed time-domain FLIM systems [13–20] and high-speed frequency-domain FLIM algorithms and systems [21–27]. In the past, rapid lifetime determination methods (RLD) were thought to be the simplest algorithms [16], and were used in some previously reported video-rate FLIMs [13,17] either with optomechanically or electronically controllable delays. To further achieve compactness for system-on-chip, we can exploit configurable devices such as field programmable gate arrays (FPGAs) to realize real-time FLIM systems. FPGAs have benefited significantly from the advances of CMOS technology. Latest FPGAs contain over hundreds millions of transistors and can easily accommodate the output signals from SPAD arrays of growing size. With the ability of configuration, designers can easily reconfigure FPGAs by hardware description language (HDL) to perform any application-specific logic functions such as lifetime calculations. We therefore evaluated the possibility of applying RLD either on-chip or on-FPGA and concluded that RLD can be implemented on FPGA with look-up tables of natural logarithmic [18] or other functions if overlap gating techniques are used [18,19]. The delay control of RLD can be easily reconfigured by users, and we expect that the system can benefit greatly from the user-friendly features. However, building a look-up table on-FPGA covering a wide range of lifetimes is inefficient and it is desirable to develop more FPGA-

#123554 - $15.00 USD Received 12 Feb 2010; revised 22 Mar 2010; accepted 22 Mar 2010; published 3 May 2010

friendly algorithms that use only additions. The impact will be especially large when applied to a massive SPAD array. Moreover, with in-pixel time-to-digital converters (TDCs) providing temporal information and flexibility [9], we therefore proposed a more hardware-friendly algorithm (on-FPGA or even on-chip) for lifetime calculations. The IEM-based system allows minimum software calculation requirements on both scanning and wide-field systems. The best way is to make the system selectable and controllable by end users. The main role of high-speed IEM algorithms is for exploratory biological experiments by adapting a wide-field microscope to accommodate the SPAD array. More precise measurements on a scanning system [4] using IEM or software can follow if necessary.

In this paper, we first derive the theory of the modified IEM FPGA implementations. The theory allows optimization of hardware usage, accuracy, and lifetime resolvability range. The FPGA implementation and Verilog hardware modeling of IEM will then be introduced, and the performance of the proposed algorithm will be tested on a variety of test samples, including various standard fluorophores, microfluidic mixing of fluorophore solutions, and living spores of *Neurospora Crassa* with a new low dark count SPAD plus 10-bit TDC array in 0.13μm CMOS technology [7,9].

2. Modified IEM FPGA implementation algorithm

As shown in [14], we can assume the fluorescence decay function $f(t) = \mathrm{A}\exp(-t/\tau)$ with τ being the lifetime when the ratio of the full width at half maximum (FWHM) of the instrumental response function (IRF) over the lifetime is much less than 1.

$$\frac{\tau_{IEM}}{h} \cong \frac{\sum_{j=0}^{M-1} C_j N_j}{N_0 - N_{M-1}}$$

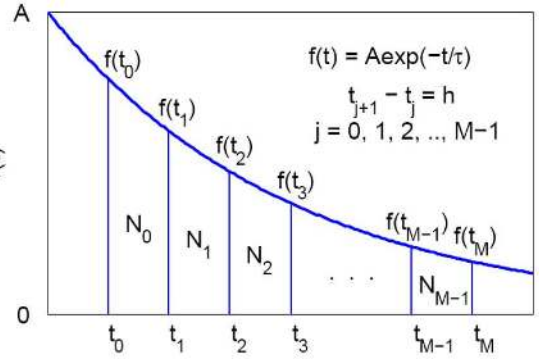

Fig. 1. Concept of IEM algorithm. The decay of a molecule is discretized in time and for each time slot the corresponding photon count is measured, approaching for large values of M the decay function $f(t)$.

For the usual measurement setup in a lab, the FWHM of the IRF is of the order of hundreds of picoseconds so it is reasonable to target lifetimes greater than 1ns. Figure 1 shows a fluorescence histogram to illustrate the concept of IEM. With M time bins (bin width of h) generated by the TDCs in the photon counting module and with the assumption of single-exponential decay, the lifetime τ is related to the decay function as

$$\frac{\tau_{IEM}}{h} \cong \frac{\sum_{j=0}^{M-1} C_j N_j}{N_0 - N_{M-1}} = \frac{N_c - (N_0 + N_{M-1})/2}{N_0 - N_{M-1}}, \quad (1)$$

where $\mathbf{C}_j$ ($\mathbf{C}_j$ = [1/3, 4/3, 2/3,…, 4/3, 1] in Ref [14], and $\mathbf{C}_j$ = [1/2, 1,…, 1, 1/2] here.) are integration coefficients, N_j (j = 0,..., M–1) is the number of counts in the jth time bin, and N_c is the total effective signal count. A hardware implementation of Eq. (1) for a single-detector sensing system was first introduced in Ref [15]. by choosing

$$N_0 - N_{M-1} = 2^L, \ L \text{ is an integer}, \quad (2)$$

#123554 - $15.00 USD Received 12 Feb 2010; revised 22 Mar 2010; accepted 22 Mar 2010; published 3 May 2010

and right-shifting the register that stores the numerator of Eq. (1) by L bits. The hardware implementation of Eq. (1) is simple because only addition and subtraction are needed. For low light situation, the histogram is almost white and $N_0 \sim N_{M-1}$, and this condition is easily avoided in hardware/software implementation. For example, end-users can set a photon count rate (PCR) threshold PCR_{th} and when the PCR is less than PCR_{th}, the system will display a black pixel on the screen.

Using IEM we assume that the timing jitter of the TDCs with phase-locked loops is negligible [14]. The insensitivity of IEM to background has been proven, and we have applied IEM to noisy SPAD pixels to demonstrate its performance and potential for sensing applications [15]. With the latest developed low dark count SPADs [7] (a dark count rate of 25Hz was reported in room temperature with a quantum efficiency of 28%), the background can be neglected for IEM. The accuracy and precision of the IEM using Eq. (1) are

$$\begin{cases} \dfrac{\Delta\tau_{IEM}}{\tau_{IEM}} = \dfrac{1}{12}\left(\dfrac{h}{\tau}\right)^2, \\ \dfrac{\sigma\tau_{IEM}}{\tau_{IEM}} = \dfrac{2}{\sqrt{N_c}}\left[1+\dfrac{1}{12}\left(\dfrac{h}{\tau}\right)^2\right]\sqrt{\dfrac{\left(1-x^M\right)\left(x+x^M\right)}{(1-x)\left(1-x^{M-1}\right)^2(1+x)^2}}, \end{cases} \tag{3}$$

where $x = \exp(-h/\tau)$. From Eq. (2), we can express N_c in term of L as

$$N_c = 2^L \frac{1-x^M}{(1-x)\left(1-x^{M-1}\right)} \cong \frac{2^L}{h}\tau. \tag{4}$$

From Eq. (4), although the hardware implementation is simple, using Eq. (2) results in the total count being lifetime-dependent, which means it takes more time to update the longer lifetimes, and therefore limits the lifetime resolvability range for real-time applications. To solve this problem, we can use the other options which we will explain later. Replacing Eq. (4) into Eq. (3), we obtain

$$\frac{\sigma\tau_{IEM}}{\tau_{IEM}} = \frac{1}{2^{L/2-1}}\left[1+\frac{1}{12}\left(\frac{h}{\tau}\right)^2\right]\sqrt{\frac{\left(x+x^M\right)}{\left(1-x^{M-1}\right)(1+x)^2}}. \tag{5}$$

Figure 2(a) shows the precision and accuracy curves for 1024-bin IEM with L = 10. The theoretical results marked as solid curves are compared with Monte Carlo simulations marked with open circles, giving good agreement. The precision curve of Eq. (5) has a flat and wide response for its optimal window from Mh/τ = 2 to 400 before it meets up the accuracy curve. From Eq. (5), the precision in the optimal window can be approximated as

$$\text{Precision} \cong 20\log\left[\frac{2^{L/2}(1+x)}{2\sqrt{x}}\right] \cong 3L \text{ (dB)}, \tag{6}$$

which is an interesting result and it allows end-users to easily set the precision of images. The bin width h is controlled by the in-pixel TDCs [9], such that h can be 50ps or 160ps. Taking h = 160ps and M = 1024 as an example, the lifetime resolvability range for a precision of 30dB is 0.41ns < τ < 82ns, which covers a large range of biological samples. The lower bound is also limited by the FWHM of the IRF response. If the IRF response is considered, the lifetime resolvability range is 1ns < τ < 82ns. Our target is to analyze samples from 1ns to 20ns, and the margin is enough considering non-idealities in the system [14].

As stated earlier, to avoid lifetime-dependent update rate, we can instead set the numerator of Eq. (1) as

#123554 - $15.00 USD Received 12 Feb 2010; revised 22 Mar 2010; accepted 22 Mar 2010; published 3 May 2010

$$N_c - \left(N_0 + N_{M-1}\right)/2 = 2^C,\ C \text{ is an integer.} \quad (7))$$

When the condition of Eq. (7) is met, only the photon count of $N_0 - N_{M-1}$ is sent out to PC for lifetime calculations. From Eq. (7) we have

$$N_c = \frac{2^{C+1}\left(1-x^M\right)}{\left(1+x\right)\left(1-x^{M-1}\right)} \approx 2^C, \quad (8))$$

$$\frac{\sigma\tau_{IEM}}{\tau_{IEM}} = \frac{2}{2^{\frac{C+1}{2}}}\left[1+\frac{1}{12}\left(\frac{h}{\tau}\right)^2\right]\sqrt{\frac{\left(x+x^M\right)}{\left(1-x\right)\left(1+x\right)\left(1-x^{M-1}\right)}} = g\left(C,\tau\right). \quad (9))$$

From Eq. (8), the total count is a weak function of x and mainly determined by C, and the lifetime update rate is mainly determined by the intensity of the fluorescent emission. Again, in this mode, a threshold PCR_{th} can be also set to display black pixels. Figure 2(b) shows the precision and accuracy curves for 256- and 1024-bin IEM with C = 14. For the numerator of Eq. (1) to collect a total count of 2^{14} in a fixed measurement window, the resolvability range for a precision larger than 20dB for M = 256 (h = 0.64ns) and M = 1024 (h = 0.16ns) are 0.55ns < τ < 82ns and 0.16ns < τ < 27ns, respectively. For real-time imaging purposes, this promises an acceptable accuracy for a wide range of lifetimes, although the accuracy is a function of lifetime. If samples with large lifetime difference co-exist and they are not stationary, this fixed total count mode works better than the previous fixed accuracy mode. To alter the resolvability range, users can change M and h via a graphical user interface (GUI).

There is another option that the FPGA can send both the numerator and denominator of Eq. (1) at a given frame update rate to PC for lifetime calculations.

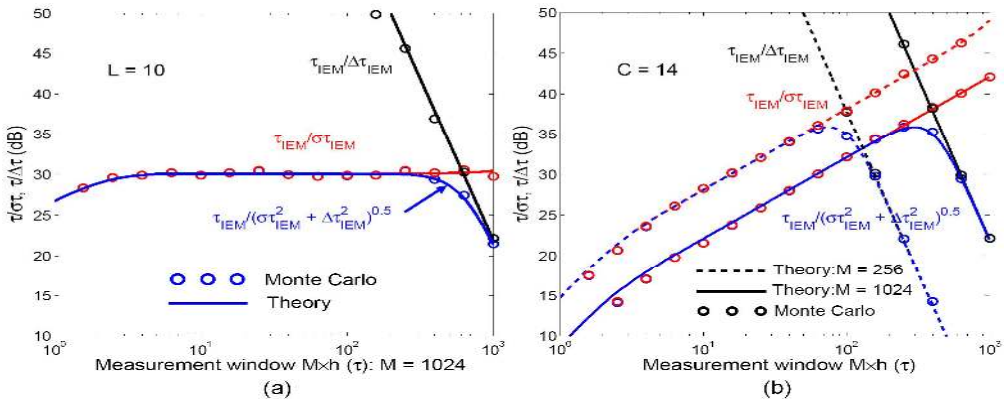

Fig. 2. Precision and accuracy curves versus measurement window in τ for the M-bin IEM with (a) a fixed denominator (L = 10) and (b) a fixed numerator (C = 14) of Eq. (1).

#123554 - $15.00 USD Received 12 Feb 2010; revised 22 Mar 2010; accepted 22 Mar 2010; published 3 May 2010

3. Modeling of IEM with hardware description language (HDL)

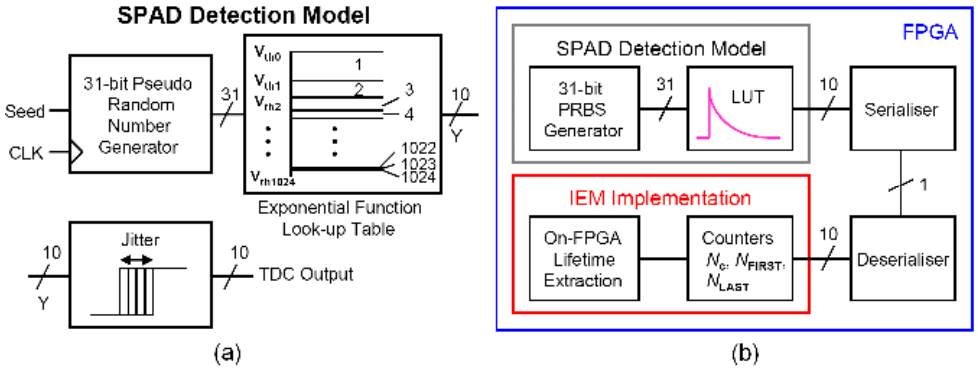

Fig. 3. (a) SPAD detection model and (b) IEM implementation on FPGA for a single SPAD.

Before employing IEM to the SPAD array, we first built a detection model of a SPAD pixel in order to verify the efficiency of the algorithm on the FPGA. Figure 3(a) and (b) show the diagrams for the SPAD detection model and the IEM implementation for a SPAD pixel, respectively. The 10 bits signal coming from a TDC in a SPAD pixel cell can be modeled by a 31-bit pseudo-random bit sequence (PRBS) generator and a look-up table used for generating a photon emission probability function. Considering the hardware usage on FPGA, we can also choose a 28-bit or a 29-bit PRBS, but the length of the 31-bit PRBS provides a more accurate model. The SPAD detection model then feeds the output data into a serializer and a deserializer to model the signal coming from the SPAD array and into the FPGA. The polynomial for generating the 31-bit PRBS is $g(x) = 1 + x^{28} + x^{31}$ [28]. The maximum length of the bit sequence is $2^{31} - 1 = 2.15 \times 10^9$, which is much larger than the total photon count of usual TCSPC measurements for a single pixel. Fixed total count scheme Eq. (7) is employed in the modeling. For comparison with RLD algorithms, we built a look-up table of digital division inside the IEM implementation block. Taking two single decay functions $f(t) = A\exp[-t/(200h)]$ and $f(t) = A\exp[-t/(10h)]$ as examples, look-up tables for such decays including the overall jitter of SPAD and laser (about $2h$ in order), pixel dark count noise, and the laser excitation delay between the electrical excitation signal and laser pulse is built right after the 31-bit PRBS generator. If h is of 160ps, the full range of the TDC is $1024h$ = 163.8ns, which is equivalent to a laser repetition rate of 6.1MHz. The lifetimes $\tau = 200h$ = 32ns and $\tau = 10h$ = 1.6ns, and since our target is to resolve τ values greater than 1ns, a typical jitter of $2h$ = 320ps can be tolerated even though only tail-fitting is applied to extract the lifetime without digital de-convolution [14]. Unlike the perfect exponential histogram shown in Fig. 1 ($FIRST = 0$, $LAST = M - 1$), the first and last channel numbers $FIRST$ and $LAST$ are 81 and 1023, respectively. Figure 4(a) and (b) shows the decay histograms N_r obtained by the model and the fitted curves N_f by IEM with background correction for $\tau = 200h$ and $\tau = 10h$ respectively. The calculated lifetimes with 4 extra bits for decimal accuracy obtained by IEM and RLD without background correction are also listed. The lifetimes obtained by MLE [10] for comparison are also listed. For RLD, its optimal measurement window is $1\tau < 2w_g < 6\tau$ [16], where w_g is the gate width, and it is a challenging task to resolve lifetimes much less than the effective measurement window ($\tau << (LAST - FIRST)h = 942h = 2w_g$ in the second case). It cannot obtain correct lifetimes using RLD either with or without background correction. For MLE, the background correction is required for the second case. However, for IEM, it has superior resolvability range and is much more insensitive to background noise. Figure 4(a) and (b) also show the normalized residual counts of $(N_r - N_f)/N_f^{1/2}$ which are well distributed, implying that the model is Poisson distributed as in real cases.

#123554 - $15.00 USD Received 12 Feb 2010; revised 22 Mar 2010; accepted 22 Mar 2010; published 3 May 2010

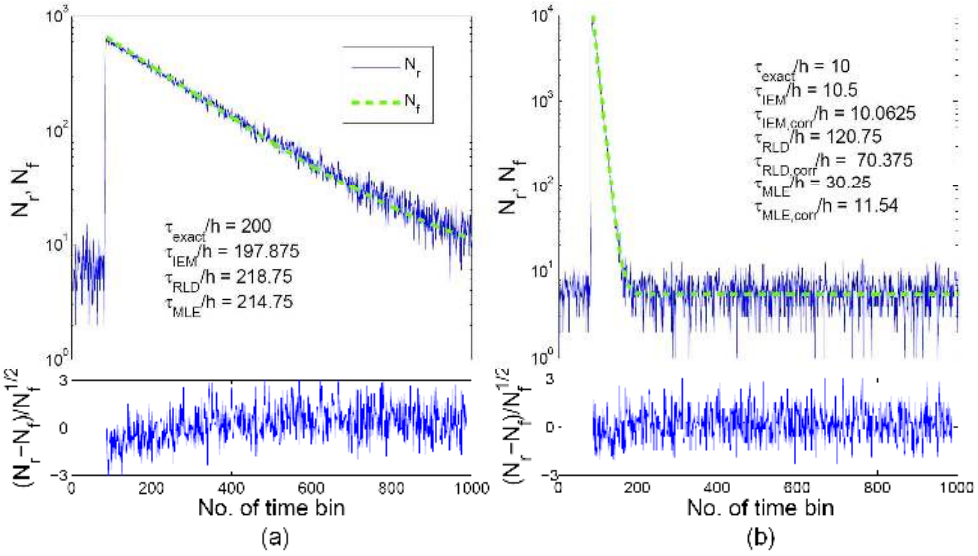

Fig. 4. Decay and fitted curves obtained by the HDL model and IEM for (a) $\tau = 200h$ and (b) $\tau = 10h$.

4. Integration of IEM with low noise CMOS SPAD arrays

Now we integrate the lifetime extraction block with a 32 × 32 SPAD pixel array (split into two 32 × 16 SPAD arrays with h = 50ps and h = 160ps). Each SPAD pixel contains a 10-bit TDC, and for each column there is a serializer to minimize the pad number. The details of the SPAD chip and in-pixel TDCs were reported in Ref. 9. The SPAD array is capable of generating data at a frame rate over 500kHz. Figure 5 (a) illustrates how the lifetime extraction algorithm works with the existing SPAD array on FPGA. First the serial data is deserialized and the output data (10-bit for each column) is connected to a housekeeper to be normalized to a format required by the IEM. The lifetime extraction module has two extra control signals *FIRST* and *LAST* sent from the GUI via USB connection. These two numbers can be generated automatically by locating the peak of the histogram during the measurement setup and characterization phase. After they have been acquired, the system starts lifetime calculations. From Eq. (1), two registers are required to store the denominator $N_{FIRST} - N_{LAST}$

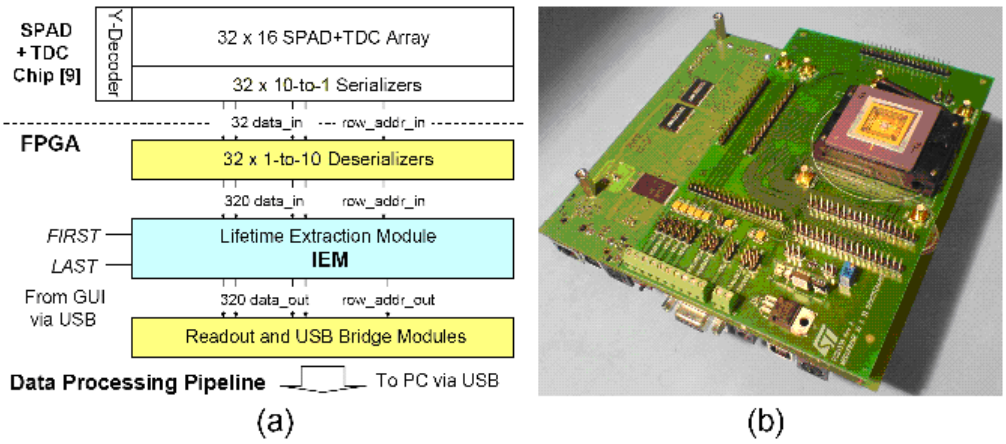

Fig. 5. (a) IEM FPGA implementation and data path (b) Imager assembly on an EPFL LASP motherboard.

#123554 - $15.00 USD Received 12 Feb 2010; revised 22 Mar 2010; accepted 22 Mar 2010; published 3 May 2010

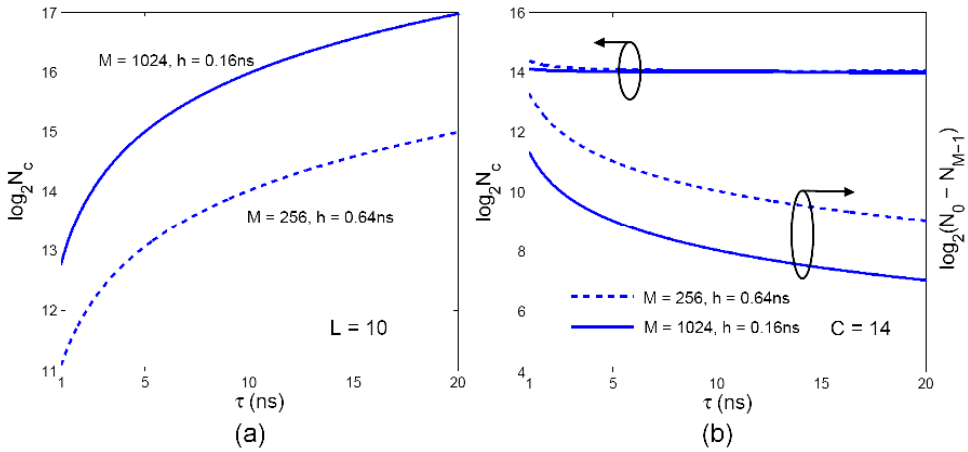

Fig. 6. Number of bits required to store N_c for (a) fixed accuracy mode and (b) fixed total count mode.

and the numerator respectively. Figure 5(b) shows the imager assembly on an EPFL LASP motherboard containing two Xilinx Virtex-II Pro FGPAs. Figure 6(a) and (b) show the number of bits required for the register to store N_c in two different modes. The GUI allows end users to set the parameters L, C, M, and h for fixed accuracy or fixed total count update. For the former mode, it takes more time to update longer lifetimes, whereas for the later mode, there is an optimized accuracy at $h \approx 0.3\tau$. To reach real-time imaging, a lower C (or L) with a higher h can be chosen with averaging and filtering functions implemented for image enhancement. The extracted lifetime, the counts N_c, and ($N_{First} - N_{Last}$) are stored in on-FPGA memory. The IEM block only uses 11% of 4-input look-up tables and 1,248 16 × 1 RAMs (= 20k bits) of a Virtex-II Pro FPGA.

5. Experimental results

For experimental demonstration of the proposed IEM hardware lifetime calculation algorithm, a fluorescence lifetime imaging system was set up on a Nikon TE2000U inverted microscope as shown in Fig. 7. A PicoQuant pulsed diode laser with a wavelength of 470nm coupled through the epi-fluorescence port of the microscope was used as excitation source. The sample was imaged onto the 32 × 32 SPAD camera prototype. Because of the small active area of the array (1.6mm^2) most images presented here used a de-magnifying image relay to achieve a reasonably large field of view. The laser pulse rate is 20MHz (when applied to the 32 × 16 array with h = 160ps, the TDC range is not fully employed and there is a stop signal for the TDC to define a proper range), and the maximum power reaching the back focal plane of the objective is about 90μW. The lifetime estimates are calculated on the camera's motherboard and then passed to a GUI on the computer via a USB link.

To test the performance of the system, glass capillaries filled with Rhodamine 6G in water (100μM) were imaged at different laser intensities. This should yield a uniform fluorescence lifetime throughout the field of view, despite the fact that there were some intensity differences due to slightly uneven illumination of the sample. The accuracy was estimated from the mean value and standard deviation of the lifetime estimates across the whole field of view. The detector's dynamic range and update rate were tested and by changing the intensity of the excitation light. In Table 1, the excitation laser power is varied from 87μW to 1.8μW, and the measured photon count rate decreases accordingly from 109kHz down to 2.1kHz, whereas the lifetime update time increases from 0.5 to 20.3 seconds. The SNR ($\tau_{ave}/\sigma\tau$ in dB) in most cases is larger than 23dB. These results are obtained without micro-lenses mounted on the camera prototype.

#123554 - $15.00 USD Received 12 Feb 2010; revised 22 Mar 2010; accepted 22 Mar 2010; published 3 May 2010

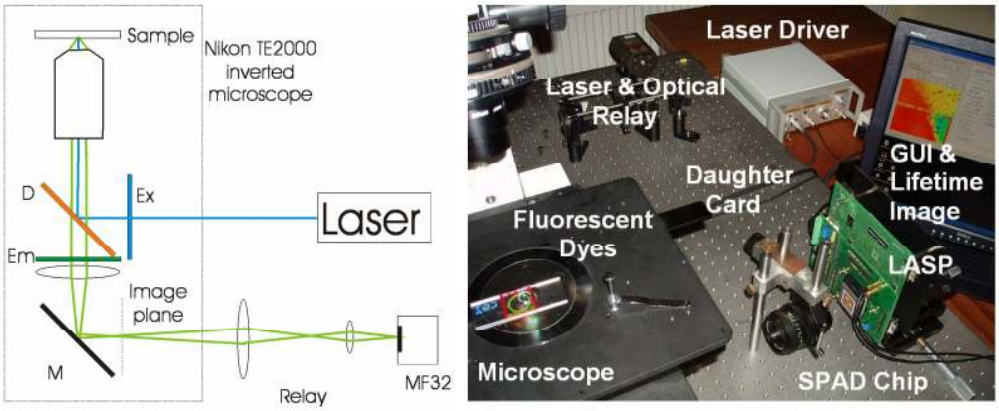

Fig. 7. Schematic and photo of the experimental setup. A standard Nikon B2-A filter cube was used for the fluorescence imaging.

Table 1. Lifetime estimates obtained from a uniform sample of Rhodamine 6G in water at a concentration of 100uM (literature lifetime τ = 4.1ns), imaged using a Nikon Plan Fluor 20x, N.A. 0.5 objective.

Excitation laser power [μW]	Photon count rate [kHz]	Lifetime τ_{ave} [ns]	Standard deviation $\sigma\tau$ [ns]	SNR $\tau_{ave}/\sigma\tau$ [dB]	Time for lifetime estimate to appear [s]
87	109.0	4.0	0.2	26	0.5
24	26.3	4.1	0.2	26	2.1
4.4	5.7	4.1	0.2	26	6.5
1.8	2.1	4.0	0.3	23	20.5

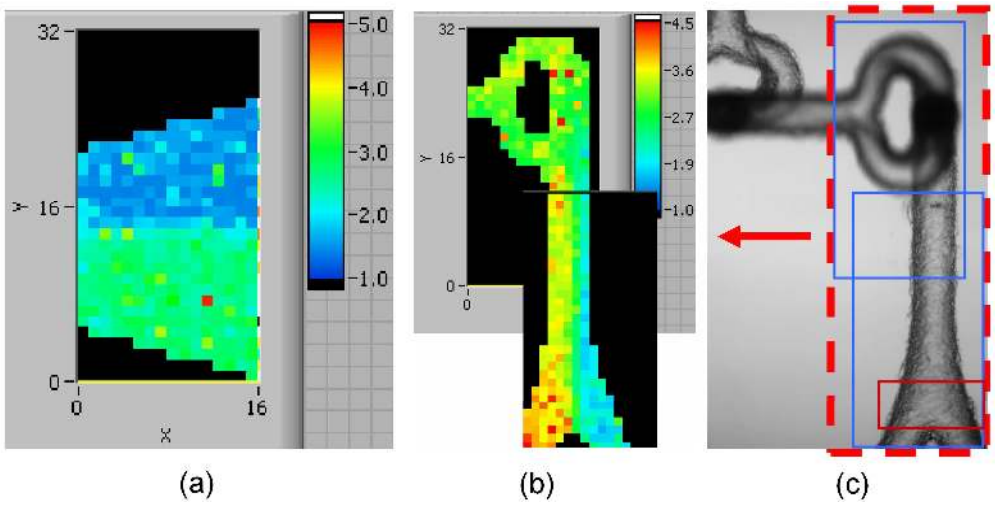

Fig. 8. Microfluidic mixing of fluorophore solutions. (a) Rhodamine B in water and ethanol (both 100μM) come together at a junction at a high flow rate (50 μl/min). (b) Interface between the two streams (here 100μM Rhodamine B and 20μM Rhodamine 6G in water) dissolves as they mix along the channel. (c) Brightfield image of the microfluidic micromixer chip (Micronit Microfluidics, FC_TD26).

The diameter of the SPAD active area is 8μm, and the pixel pitch is 50μm [9]. Due to the in-pixel circuitry for recording raw arrival-time information, the fill factor is only 2%, and a

#123554 - $15.00 USD Received 12 Feb 2010; revised 22 Mar 2010; accepted 22 Mar 2010; published 3 May 2010

microlens array is therefore desirable for focusing the light. A microlens array fabricated on the imager was reported and can be employed to further boost the lifetime update rate more than 10-fold [29], making it promising for real-time applications. Lifetimes have been obtained for Rhodamine B (τ = 1.7ns) and Rubrene (τ = 8.1ns, this lifetime value differs from the reported literature value of τ = 9.9ns due to oxygen quenching, but was confirmed by independent measurements in an Edinburgh Instruments FL920 fluorescence lifetime spectrometer.) in water and quantum dot samples ($\tau \approx$16ns, measured at lower laser repetition rate), confirming that the system performs well over a wide range of typical fluorescence lifetimes. The current camera thus provides 32 × 16 parallel lifetime calculations at very high speed and high accuracy.

To demonstrate that the IEM algorithm in conjunction with the detector array can visualize lifetime changes in 'real time' a microfluidic mixing experiment has been set up [12]. Microfluidic flow cells were used to combine and mix two solutions of fluorophores, driven through the systems at a constant flow rate by use of a syringe pump. At high flow rates the two streams form a sharp interface close to the junction (see Fig. 8(a)) and the small lifetime difference of Rhodamine B due to the solvent (water in the upper channel and ethanol in the lower channel) is clearly visualized, with mean lifetime estimates in agreement with literature values (1.6ns and 2.6ns, respectively). The lifetime estimates are updated about 7 times a second (L = 10). If L is reduced to 9, the lifetime update rate can be 14Hz with an acceptable accuracy, making it possible to monitor changes to the flow (e.g. if one channel is blocked) in real time. With a micro-lens array [29] mounted, the update rate can be further increased. Figure 8(b) shows a lower magnification image of 100μM Rhodamine B and 20μM Rhodamine 6G (both in water) coming together in a microfluidic micromixer chip (see Fig. 8(c)) at a slow flow rate. Initially the flows can be clearly distinguished due to their lifetime difference but further down the channel they mix due to diffusion of the fluorophores, as visualized by the uniform intermediate lifetime further down the channel. Figure 9 (Media 1) shows dynamic changes in the flow of the same combination of fluorophore solutions in a home-made T-mixer flow cell. The flow has been stopped before the movie recording was started, leading to a diffuse interface between the two solutions. As the flow in both channels is re-started the interface sharpens, demonstrating that the detector in combination with IEM can monitor changes in fluorescence lifetime in real-time.

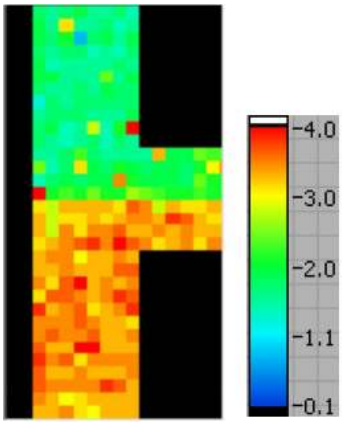

Fig. 9. (Media 1) Interface between two streams (100μM Rhodamine B from top inlet and 20μM Rhodamine 6G in water from the bottom inlet) changes as the flow rate is varied in a T-mixer (dimensions: W400μm × H200μm). Media at 5 times the actual speed (104s in real time): Initially the flow had been stopped, the flow was then re-started at time 5s, leading to a sharp interface between 2 well distinguished streams, but start to mix again after the flow has been stopped at time 45s.

#123554 - $15.00 USD Received 12 Feb 2010; revised 22 Mar 2010; accepted 22 Mar 2010; published 3 May 2010

Figure 10 shows lifetime data obtained from living fungal spores. *Neurospora Crassa* has been genetically modified to express Green fluorescent protein (GFP) and was imaged in a set-up similar to Fig. 7 but without the demagnifying image relay. Use of a high magnification oil immersion objective (Nikon Plan Apo 100 × , N.A. 1.4) yields a field of view of 16 μm × 8μm. The low photon detection efficiency of the current SPAD device led to a rather low photon count rate in fluorescence mode, but nevertheless lifetime estimates are available after about 9s. For lifetime sensing purposes, the camera provides 32 × 16 parallel lifetime calculations and offers very high speed and high accuracy detection. Although the resolution of the camera prototype is still low, the lifetime calculation algorithm is proven feasible, and its on-chip implementation on a larger CMOS SPAD array with microlenses recovering the fill factor is coming soon.

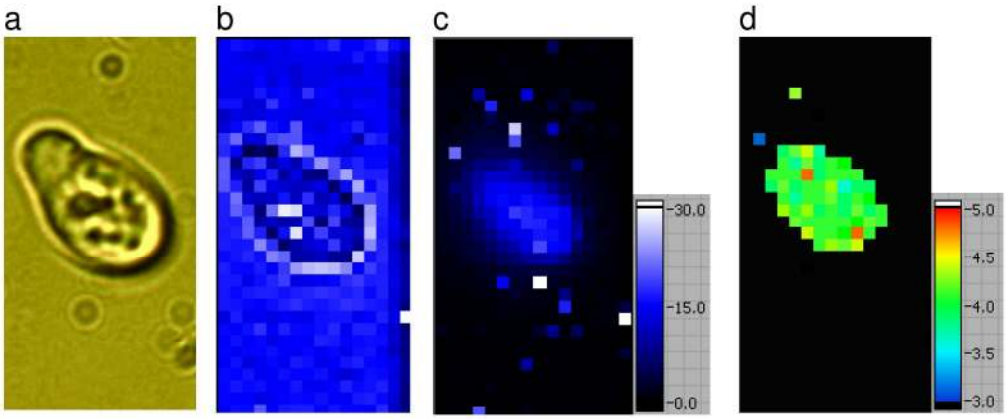

Fig. 10. Images of fungal spores (Neurosporra crassa) which have been genetically modified to express GFP. Brightfield image on (a) standard CCD and (b) 32 × 16 SPAD array (c) Fluorescence intensity image (scale indicating photon count rate in kHz) and (d) Lifetime image indicating a uniform lifetime of about 4ns throughout the spore. Field of view 8 μm × 16 μm.

6. Conclusion

A newly proposed integration based algorithm IEM for real-time FLIM systems has been successfully implemented on FPGA. A photon detection model for single SPAD is proposed to verify the accuracy and efficiency of the algorithm. With a 0.13μm CMOS 32 × 32 SPAD array, IEM can work in parallel for each pixel and the calculated lifetime is updated at a certain condition dictated by Eqs. (2) or (7) for fixed accuracy or fixed total count modes. A widefield microscope was adapted to accommodate the array and test it on biological applications. Without resorting to slow software analysis tools, the real-time image allows instantaneous monitoring of bio-chemical interactions to provide quick feedback for corresponding manipulations. The FLIM prototype successfully updates the lifetime image within tens of milliseconds. The error is greatly reduced after introducing new low dark count SPADs into the imager. With micro-lens mounted on the SPAD in the future, the camera can be further employed to single molecule detection. To the best of our knowledge, this is the first FLIM system-on-chip using low dark count CMOS SPAD detectors [7,9] that can generate real-time fluorescence lifetime images. The usage of hardware resource for implementation is small thanks to the simplicity of Eqs. (1). With this merit, IEM can be even implemented in-pixel for further image compression and reduced I/O bandwidth. Along with integrated excitation sources such as low cost, high speed LED arrays [8], this prototype system promises low-cost, miniaturized fluorescence lifetime imaging and sensing for portable instrumentation.

#123554 - $15.00 USD Received 12 Feb 2010; revised 22 Mar 2010; accepted 22 Mar 2010; published 3 May 2010

Acknowledgments

This work has been supported by the European Community within the Sixth Framework Programme of the Information Science Technologies, Future and Emerging Technologies Open MEGAFRAME project (contract 029217-2, www.megaframe.eu). We acknowledge the support from the Scottish Funding Council for the Joint Research Institute with the Heriot-Watt University which is a part of the Edinburgh Research Partnership in Engineering and Mathematics (ERPem). The system has been built with help from Lucio Carrara and Theo Kluter, EPFL. The measurements have been performed using the COSMIC laboratory facilities with help from Robin Andrews, Gerard Giraud, Ondrej Nenadl, Trevor Whittley, and David Dryden. The authors would like to express gratitude to them as well as Nick Read and Alexander Lichius for providing fungal spores for imaging. This publication reflects only the authors' views. The European Community is not liable for any use that may be made of the information contained herein.

#123554 - $15.00 USD Received 12 Feb 2010; revised 22 Mar 2010; accepted 22 Mar 2010; published 3 May 2010